Six-week time series of eddy covariance CO_2 flux at Mammoth Mountain, California: performance evaluation and role of meteorological forcing

J.L. Lewicki[a*], M.L. Fischer[b], G.E. Hilley[c]

[a*]*Earth Sciences Division, Ernest Orlando Lawrence Berkeley National Laboratory, Berkeley, CA, USA 94720, e-mail: jllewicki@lbl.gov, ph: 510-495-2818, fax: 510-486-5686*

[b]*Environmental Energy Technology Division, Ernest Orlando Lawrence Berkeley National Laboratory, Berkeley, CA, USA 94720, e-mail: mlfischer@lbl.gov*

[c]*Department of Geological and Environmental Sciences, Stanford University, Stanford, CA, USA 94305, e-mail: hilley@pangea.stanford.edu*

Abstract

CO_2 and heat fluxes were measured over a six-week period (09/08/2006 to 10/24/2006) by the eddy covariance (EC) technique at the Horseshoe Lake tree kill (HLTK), Mammoth Mountain, CA, a site with complex terrain and high, spatially heterogeneous CO_2 emission rates. EC CO_2 fluxes ranged from 218 to 3500 g m^{-2} d^{-1} (mean = 1346 g m^{-2} d^{-1}). Using footprint modeling, EC CO_2 fluxes were compared to CO_2 fluxes measured by the chamber method on a grid repeatedly over a 10-day period. Half-hour EC CO_2 fluxes were moderately correlated (R^2 = 0.42) with chamber fluxes, whereas average-daily EC CO_2 fluxes were well correlated (R^2 = 0.70) with chamber measurements. Average daily EC CO_2 fluxes were correlated with both average daily wind speed and atmospheric pressure; relationships were similar to those observed between chamber CO_2 fluxes and the atmospheric parameters over a comparable time period. Energy balance closure was assessed by statistical regression of EC energy fluxes (sensible and latent heat) against available energy (net radiation, less soil heat flux). While incomplete (R^2 = 0.77 for 1:1 line), the degree of energy balance closure fell within the range observed in many investigations conducted in contrasting ecosystems and climates. Results indicate that despite complexities presented by the HLTK, EC can be reliably used to monitor background variations in volcanic CO_2 fluxes associated with meteorological forcing, and presumably changes related to deeply derived processes such as volcanic activity.

Keywords: CO_2 emissions; volcano monitoring; eddy covariance; chamber method; Mammoth Mountain

1. Introduction

The measurement of surface emissions of CO_2 has become an integral part of many volcanic and geothermal monitoring programs, as temporal variations in emissions may indicate changes at depth associated with volcanic activity or geothermal processes (e.g., Baubron et al., 1991; Farrar et al., 1995; Chiodini et al., 1998; Hernandez et al., 1998; Klusman et al., 2000; McGee et al., 2000; Bergfeld et al., 2001; Hernandez et al., 2001; Werner and Cardellini, 2006). Furthermore, it is important to understand the link between temporal variations in deeply derived CO_2 emissions, and meteorologic and hydrologic processes, as these near-surface processes can drive large changes in CO_2 emissions (e.g., Connor et al., 1993; McGee and Gerlach, 1998; Rogie et al., 2001; Granieri et al., 2003; Lewicki et al., 2007) that may pose health and environmental hazards or be misinterpreted to reflect changes at depth.

While the chamber method (e.g., Chiodini et al., 1998) has been reliably used to measure spatial and temporal variations in surface CO_2 fluxes in many volcanic and geothermal regions, limitations of the method include the measurement's small spatial scale (<1 m^2), alteration of the ground surface and gas flow during the measurement, and the ability to continuously monitor temporal changes in CO_2 fluxes at only a single or limited number

66 of point locations within a study area. The eddy covariance (EC) method, a
67 micrometeorological technique traditionally used to measure CO_2 (and other trace gas
68 and heat) fluxes across the interface between the atmosphere and a plant canopy (e.g.,
69 Baldocchi, 2003 and references therein) has been proposed as a viable and
70 complementary technique to monitor volcanic CO_2 and heat fluxes in conjunction with
71 the chamber method (Werner et al., 2000; 2003; 2006; Anderson and Farrar, 2001). EC
72 provides the benefit of an automated flux measurement that does not interfere with the
73 ground surface and is averaged over both time and space, with the spatial scale
74 significantly larger (m^2-km^2) than that of the chamber method. Importantly, however, the
75 theory that underlies the EC method assumes spatial homogeneity of surface fluxes, flat
76 terrain, and temporal stationarity (e.g., Folken and Wichura, 1996), conditions that are
77 not typically met in volcanic and geothermal environments.
78
79 Work in mountain ecosystems has shown that under suitable atmospheric conditions, EC
80 can provide reliable CO_2 and heat flux measurements in complex terrain (e.g., Turnipseed
81 et al., 2003; 2004). Werner et al. (2000; 2003) deployed EC from 1 to 2.5 weeks in the
82 Yellowstone National Park hydrothermal system, USA and at Solfatara volcano, Italy,
83 sites with highly heterogeneous surface CO_2 and heat fluxes, yet relatively flat terrain.
84 Using footprint modeling, they showed general consistency between EC CO_2 fluxes and
85 chamber CO_2 fluxes measured on grids, indicating that EC yielded representative
86 measurements at these sites. However, Werner et al. (2003) suggested that the relative
87 difference observed between the two methods could have been derived in part by
88 incomplete characterization of the temporal variability of surface CO_2 fluxes within the

89 study area by the chamber method over the EC measurement period. Anderson and
90 Farrar (2001) performed EC measurements of CO_2 and heat fluxes for up to four days in
91 three pilot studies at the Horseshoe Lake tree kill (HLTK) on Mammoth Mountain, USA
92 (Figure 1). The HLTK is a site with complex terrain and highly heterogeneous, yet cold
93 volcanic CO_2 emissions, thus possessing distinctly different characteristics from the
94 Yellowstone and Solfatara areas. While they found average EC CO_2 flux measurements
95 to be generally similar to chamber measurements made in separate studies, footprint
96 modeling as performed by Werner et al. (2000; 2003) would have been required to
97 directly compare the results derived from these two methods.
98
99 We build on the work of Werner et al. (2000; 2003) and Anderson and Farrar (2001) by
100 presenting a six-week time series of EC CO_2 fluxes measured at the HLTK. We assess
101 the quality of EC CO_2 and heat flux measurements by comparing them to measurements
102 made by independent techniques. In particular, EC CO_2 fluxes were compared to
103 chamber CO_2 fluxes over a 10-day period when spatio-temporal variations in surface CO_2
104 fluxes were captured by repeated chamber measurements on a grid. Despite the
105 complexities presented by the study site, we show that under certain atmospheric
106 conditions, the EC method performs well relative to independent methods. Finally, the
107 multi-week time series of EC fluxes allowed us to establish relationships between
108 temporal variations in surface CO_2 fluxes and meteorological parameters on time scales
109 longer than a day.
110
111 **2. Study Site**

Mammoth Mountain (3368 m) is a dormant dacitic volcano formed 200,000 to 50,000 years ago on the southwestern rim of Long Valley caldera, eastern California (Figure 1). While lavas were last erupted ~50,000 years ago, phreatic eruptions occurred up to ~700 years ago (Bailey, 1989). Recent volcanic unrest associated with Mammoth Mountain was first detected in 1979 and activity was subsequently expressed as ground deformation, swarms of small earthquakes ($M \leq 3$), spasmodic bursts, long-period and very long-period earthquakes, elevated $^3He/^4He$ ratios in fumarolic gases, and diffuse surface CO_2 emissions (Hill and Prejean, 2005). An eleven-month-long seismic swarm occurred at Mammoth Mountain in 1989, possibly related to dike intrusion and/or magmatic fluid migration (Hill, 1996; Hill and Prejean, 2005). Tree kills then formed in six general areas on Mammoth Mountain in 1990-1991 due to diffuse, non-thermal emissions of volcanic CO_2 resulting in high CO_2 concentrations in the root zone (e.g., Farrar et al., 1995).

The HLTK is the largest (~120,000 m^2) tree kill on Mammoth Mountain and is located on the northwest shore of Horseshoe Lake, on the southeast flank of the volcano (Figure 1). It lies in the Lakes Basin, with terrain sloping upward to the west-northwest (Figures 1 and 2). Soils here are largely barren of vegetation, 1 to 3 m thick, and composed of 0.1 to 0.4 m of pumice overlying coarse sand with cobbles to boulders and low organic carbon (McGee and Gerlach, 1998; Evans et al., 2001). Horseshoe Lake is perched, while the water table here is located at ~40 m depth (HSL-1 well; Farrar et al., 1998).

Extensive monitoring of subsurface CO_2 concentrations and surface CO_2 fluxes has been conducted at the HLTK (e.g., Farrar et al., 1995; Rahn et al., 1996; Gerlach et al., 1998; McGee and Gerlach, 1998; McGee et al., 2000; Gerlach et al., 2001; Anderson and Farrar, 2001; Rogie et al., 2001; Lewicki et al., 2007). Studies have reported large diurnal to seasonal fluctuations in time series of soil CO_2 concentrations, surface CO_2 fluxes, and total CO_2 discharges that appear to be due to variations in meteorological and hydrologic processes (e.g., McGee and Gerlach, 1998; McGee et al., 2000; Rogie et al., 2001). Also, Lewicki et al., (2007) showed that large spatio-temporal variations in surface CO_2 fluxes over multiple days can be driven by slow-moving cold fronts. Furthermore, long-term monitoring suggests that emissions have markedly declined over the past decade. For example, the average estimated CO_2 discharge from the tree kill area was ~250 t d^{-1} for 1995 to 1997 (Gerlach et al., 1998) and 93 t d^{-1} for 1997 to 2000 (Rogie et al., 2001), whereas the average discharge measured in 2006 was 38 t d^{-1} (Lewicki et al., 2007).

3. Methods

3.1. Eddy covariance measurements

An EC station (2.5 m high; see below) was deployed at the HLTK (Figure 2) continuously from 09/08/2006 to 10/24/2006. The location of the station was chosen to take advantage of the westerly prevailing winds and the absence of asphalt road and parking lot to the west. The average surface slope to the west (from directions of 190 to

158 360^{o}) and within 100 m of the station was 9% (range = 1 to 15%; Figure 2). Within 300
159 m of the station, the average slope was 13% (range = 1 to 18%). Widely distributed tree
160 stumps, rocks, and logs were located within about 50 m of the EC station. In addition,
161 foliage-free standing dead trees, which have lost the majority of fine branches, were
162 located from about 50 to 200 m from the EC station (Figure 1).
163
164 The EC station was similar in design to that described by Billesbach et al. (2004) and was
165 composed of fast-response and slow-response subsystems. The fast-response subsystem
166 included two sensors used to measure the variables necessary to calculate turbulent fluxes
167 of CO_2, H_2O, heat, and momentum. A Gill-Solent WindMaster Pro sonic three-
168 dimensional anemometer/thermometer (Gill Instruments, Ltd) measured wind speeds in
169 three directions and sonic temperature at 10 Hz. A LI-COR 7500 open-path CO_2-H_2O
170 infrared gas analyzer (LI-COR, Inc) measured CO_2 and water vapor densities at 10 Hz.
171 Both sensors were mounted to the top of a tripod tower at 2.5 m height.
172
173 The slow-response subsystem included sensors associated with a second tripod tower that
174 measured auxiliary variables used to compare with EC fluxes and establish relationships
175 between EC fluxes and environmental parameters. Atmospheric pressure was measured
176 using a Vaisala PTB101B barometer (Vaisala, Inc.). Atmospheric temperature and
177 relative humidity were measured using a Vaisala HMP50 humidity and temperature
178 probe. Mean horizontal wind speed and direction were measured by a Climatronics
179 CS800-12 wind set (Climatronics Corp.) at 2.5 m height. Net radiation, total insolation
180 and photosynthetically active radiation (PAR) were measured with a Kipp & Zonen

CNR-1 radiometer (Kipp & Zonen), LI-COR LI-200SA pyranometer, and LI-COR LI-190SA quantum sensor, respectively, mounted to a horizontal bar extending from the tripod tower at 2 m height. Mean precipitation was measured by a TE525 tipping bucket rain gage (Texas Electronics). Soil moisture profiles (10 and 30 cm depth) were measured at two locations using ECH2O (Decagon Devices) soil moisture probes. Soil temperature profiles (10, 20, and 30 cm depth) were measured at two locations with thermocouples. Soil heat flux was measured by four HFT3 soil heat flux plates (Radiation and Energy Balance Systems) located at 5 cm depth near the radiometer. Slow-response subsystem variables were measured every 5 seconds and averaged over 30 minutes for comparison with turbulent fluxes.

Carbon dioxide, latent heat (*LE*), sensible heat (*H*), and momentum fluxes (F_s) were calculated as the temporal covariance of the scalar (*s*) and vertical wind velocity (*w):*

$$F_s = \overline{w's'} \quad (1)$$

where the overbar denotes time averaging and primes denote deviations from a mean. Fluxes were calculated for 30-minute periods. Equation 1 gives the mean vertical turbulent flux of the scalar of interest over a horizontally homogeneous surface under steady-state conditions. Details on the theory and assumptions of the EC method can be found in Baldocchi et al. (1988); Foken and Wichura (1996); Aubinet et al. (2000); Baldocchi (2003).

For each half-hour of data, the mean lateral ($\overline{v}$) and then the mean vertical ($\overline{w}$) wind velocities were rotated to zero (Kaimal and Finnigan, 1994). The Webb correction for the effects of fluctuation in heat and water vapor on the density of air (Webb et al., 1980) was applied. Raw signals from the infrared gas analyzer and sonic anemometer were evaluated for voltage spikes and all points more than ten standard deviations (thereby accepting a non-Gaussian tail to the data) away from a 60 s moving average were removed from the data. Turbulent fluxes measured during periods of insufficient turbulent mixing are typically underestimated. To filter data for this effect, friction velocities (u_*) were calculated as the square root of the momentum flux. Figure 3 shows a plot of EC CO_2 flux versus u_* for all EC measurements corresponding to mean wind directions from 190 to 360^o (i.e., hereafter, only EC measurements corresponding to mean wind directions from the tree kill area will be considered). EC CO_2 fluxes increase sharply with u_* until u_*~0.25 m s^{-1}, above which EC fluxes remain relatively constant (Figure 3). We eliminated all EC (CO_2 and heat) fluxes corresponding to $u_* \leq 0.25$ m s^{-1}. A test for stationarity was conducted according to Foken and Wichura (1995). Each 30-minute EC flux measurement was divided into six five-minute segments. If the difference between the average of the six five minute segments and the 30-minute measurement was greater than 30%, the measurement was considered non-stationary and discarded. Specific details of data filtering are also shown on each of the following figures.

3.2. Chamber measurements

227 Surface CO_2 flux was measured using a WEST Systems fluxmeter (WEST Systems)
228 based on the chamber method, with repeatability of ±10% (Chiodini et al., 1998). Evans
229 et al. (2001) conducted laboratory measurements of imposed CO_2 fluxes over a range
230 typical of Mammoth Mountain tree kill areas through a synthetic "soil" similar in
231 properties to surficial deposits in the tree kill areas, and showed that chamber
232 measurements were negatively biased, on average by 12.5%. Collars were not used for
233 chamber measurements, due to due to the potential alteration of soil properties and gas
234 flow (e.g., Gerlach et al., 2001). Surface CO_2 flux was measured at 170 grid points at 27-
235 m spacing in the HLTK (Figure 2). Flux measurements were repeated in the same order
236 along the grid each day from 09/12/2006 to 09/21/2006 between 07:00 and 15:00, with
237 the exception of 09/15/2006 when no measurements were made. For the purpose of
238 comparison with EC CO_2 fluxes, the negative bias in chamber measurements was
239 corrected for by increasing each flux measurement by 12.5%. A map of surface CO_2 flux
240 was then produced for each day of grid measurements using nearest neighbor
241 interpolation at 5 x 5 m resolution, chosen for its simplicity in the comparison of chamber
242 to EC CO_2 flux measurements. Surface CO_2 flux maps produced using the sequential
243 Gaussian simulation method and corresponding total CO_2 discharges from the study area
244 are presented in Lewicki et al. (2007). For reference, Lewicki et al. (2005) presented a
245 comparison of a range of geostatistical interpolation and simulation methods that were
246 applied to chamber CO_2 fluxes measured in a volcanic environment.
247
248 **4. Results**
249

250 *4.1. Meteorology*

251

252 Atmospheric temperatures ranged from –8.3 to 20.8^{o}C and winds were dominantly from
253 the west (Figure 4) over the study period. The highest wind speeds were measured from
254 westerly directions, while easterly winds typically corresponded to relatively low wind
255 speeds (Figure 4). Precipitation (typically light snow) occurred on six days during
256 October (10/01/2006, 10/02/2006, 10/10/2006, 10/11/2006, 10/14/2006, and 10/17/2006)
257 (Figures 5b and 7). Average daily wind speeds and atmospheric pressures varied from
258 1.1 to 3.5 m s^{-1} and 725 to 740 mbar, respectively from 09/08/2006 to 10/24/2006 (Figure
259 5a). A cold front occurred on 09/14/2006 to 09/15/2006 (Lewicki et al., 2007) and was
260 accompanied by high average daily wind speeds and low atmospheric pressures (see zone
261 I on Figure 5a). Over the entire measurement period (09/08/2006 to 10/24/2006),
262 average daily wind speeds and atmospheric pressures were moderately inversely
263 correlated (correlation coefficient = -0.43). From 09/08/2006 to 09/22/2006 (zone I,
264 Figure 5a), average daily wind speed and pressure were strongly inversely correlated
265 (correlation coefficient = -0.80). Relationships between meteorological parameters and
266 chamber CO_2 fluxes over this time period were examined in Lewicki et al. (2007). We
267 therefore selected this time frame to analyze relationships between meteorological
268 parameters and EC CO_2 fluxes for comparison. From 09/24/2006 to 10/10/2006 (zone II,
269 Figure 5a), average daily wind speed and pressure were poorly correlated (correlation
270 coefficient = 0.14). We selected zone II to examine correlations between average daily
271 wind speed, pressure, and EC CO_2 fluxes because of different meteorological conditions

(i.e., lack of a cold front) from zone I, and a sufficient number of EC data to perform the analysis.

4.2. Chamber fluxes

Large spatio-temporal variations in surface CO_2 fluxes were measured using the chamber method from 09/12/2006 to 09/21/2006 (Figures 5b and 6). During the first two days of measurements (09/12/2006 and 09/13/2006), the spatial distribution of surface CO_2 fluxes remained relatively stable (Figure 6a-b). Then, on 09/14/2006 surface CO_2 fluxes decreased and the region of relatively high flux began to contract in size (Figures 5b and 6c). On 09/16/2006, surface CO_2 fluxes continued to decrease and the region of elevated flux further contracted in size (Figures 5b and 6d). CO_2 fluxes then increased and the region of elevated CO_2 flux expanded outwards on 09/17/2006 to 09/18/2006 (Figures 5b and 6e-f). With the exception of on 09/19/2006, surface CO_2 fluxes continued to increase over the remainder of the measurement period (Figures 5b and 6g-i). Further details on the spatio-temporal variations in chamber CO_2 fluxes are found in Lewicki et al. (2007).

4.3. Eddy covariance CO_2 fluxes

EC CO_2 fluxes measured from 09/08/2006 to 10/24/2006 ranged from 218 to 3500 g m^{-2} d^{-1} (Figure 7), with a mean and standard deviation of 1346 and 575 g m^{-2} d^{-1}, respectively. Large gaps in the time series of CO_2 fluxes were present due to filtering for mean horizontal wind direction, u_*, and stationarity. For example, 47% of the EC CO_2

295 fluxes corresponding to wind directions from 190 to 360° were lost due to filtering for u_*
296 and stationarity.
297
298 *4.4. Comparison of eddy covariance to chamber CO_2 fluxes*
299
300 The vertical scalar flux (e.g., of CO_2; F_{CO2}) measured by EC at point (x_m, y_m, z_m) is the
301 integral of the contributions from all upwind surface CO_2 emissions. The relative weight
302 of each surface point source emission on F_{CO2} depends on its location relative to the EC
303 instrumentation. F_{CO2} is related to the distribution of source CO_2 fluxes at the surface (x',
304 y', $z' = z_0$) with strength Q_{CO2} by the footprint function or source weight function, $f(x_m - x', y_m - y', z_m - z_0)$:
305
306
307 $$F_{CO2}(x_m, y_m, z_m) = \int_{-\infty}^{\infty}\int_{-\infty}^{\infty} Q_{CO2}(x', y', z' = z_0)\cdot f(x_m - x', y_m - y', z_m - z_0)\cdot dx'\cdot dy' \quad (2)$$
308
309 (e.g., Horst and Weil, 1992; Schmid, 1997). The value of the footprint function generally
310 rises to a maximum some distance upwind of the EC sensors, then smoothly falls off in
311 all directions. The total surface influence on F_{CO2}, or the source area, is the integral
312 beneath the footprint function.
313
314 Similar to the methods of Werner et al. (2000; 2003), we compared EC with chamber
315 measurements of CO_2 flux by modeling the footprint function for each half-hour EC
316 measurement from 09/12/2006 to 09/21/2006. The Flux Source Area Model (FSAM) of
317 Schmid (1997), based on analytic solutions of the advection-diffusion equation (Horst

318 and Weil, 1992) was used to model footprint functions using the following inputs: (1) z_m
319 = 2.5 m; (2) surface roughness height, z_0 = 0.03 m, in accordance with Anderson and
320 Farrar (2000); (3) measured mean horizontal wind direction; (4) cross-wind turbulence
321 near the surface characterized by calculated σ_v/u_*, where σ_v is the standard deviation of
322 the wind speed in the cross-wind direction; (5) calculated Monin-Obukhov length, L, if
323 corresponded to unstable atmospheric conditions (i.e., only measurements corresponding
324 to $L < 0$ were considered) (Table 1). We calculated f at the center of each 25-m^2 grid
325 block in Figure 6. The source area was defined here as the area within which 90% of the
326 measured EC flux was derived from. Results indicated that the source area was located
327 within ~100 m upwind of the EC station for all of the 73 footprint functions modeled
328 (mean = 86 m, range = 26 to 108 m; Figure 8). In other words, the source area was
329 contained within the tree kill area for all modeled footprint functions.
330
331 On each day from 09/12/2006 to 09/21/2006, Q_{CO2} was assumed equal to the chamber
332 CO_2 flux in Figure 6. The product of Q_{CO2} and f was then calculated for each 25-m^2 grid
333 block and summed over the source area, yielding the "footprint CO_2 flux". Figure 9
334 shows a histogram of the relative difference between the measured EC CO_2 flux and the
335 footprint CO_2 flux, expressed as a percent of the EC flux. The mean relative difference
336 was –0.3%, with a standard error = 2.7%. The standard deviation of the relative
337 difference was 23% and the mode was offset positively from zero. No systematic
338 relationship was observed between the relative difference and L, u_*, time of day, or wind
339 direction for the ranges of values considered. A plot of EC versus footprint CO_2 flux
340 (Figure 10a) shows that the data were moderately correlated (R^2 = 0.42 for 1:1 line). At

CO_2 flux up to ~1300 g m^{-2} d^{-1}, the data clustered around the 1:1 line, while at higher flux, EC CO_2 fluxes tended to be biased high relative to footprint CO_2 fluxes. Mean vertical wind velocities ($\overline{w}$) corresponding to the modeled footprints ranged from -0.43 to 0.03 m s^{-1} (mean and standard deviation = -0.17 and 0.12 m s^{-1}, respectively). $\overline{w}$ was negatively correlated (correlation coefficient = -0.37) with the relative difference between the EC and footprint CO_2 fluxes, such that EC CO_2 fluxes were typically greater than footprint fluxes when $\overline{w}$ was more negative.

The correlation of average daily EC and average daily footprint CO_2 flux increased substantially (R^2 = 0.70 for 1:1 line) relative to half-hour measurements, while the positive bias at flux >1300 g m^{-2} d^{-1} was reduced (Figure 10b). Furthermore, the correlation between average daily $\overline{w}$ (Table 1) and the relative difference between EC and footprint CO_2 fluxes was reduced (correlation coefficient = 0.24) relative to half-hour measurements.

4.5. Relationships between temporal variations in EC CO_2 fluxes and meteorology

To assess the relationships between temporal variations in meteorological parameters and EC CO_2 fluxes, we calculated average daily EC CO_2 fluxes from 09/08/2006 to 10/24/2006 using fluxes corresponding to a narrow range of mean horizontal wind directions (250 to 290^o; Figure 5b). Since the source area changes for each EC flux measurement depending on atmospheric conditions, a time series of EC fluxes is influenced by both temporal variations in, and spatial heterogeneity of, surface fluxes. This spatial component can complicate comparison of temporal variations in EC CO_2

365 fluxes to meteorological (or deep volcanic, hydrothermal) processes. Therefore, to limit
366 the effects of spatial heterogeneity of surface fluxes on the evaluation of temporal
367 variability of EC CO_2 fluxes, we only considered fluxes corresponding to a narrow range
368 of mean horizontal wind directions (250 to 290^o) in the calculation of average daily EC
369 CO_2 fluxes (Figure 5b). However, in this simple analysis, it was not possible to assess
370 changes in the same flux source area over time.
371
372 No systematic relationship was observed between average daily EC CO_2 flux and average
373 daily atmospheric or soil temperature. A decrease in average daily and half-hour EC CO_2
374 fluxes was observed during precipitation events on 10/01/2007-10/02/2007 and
375 10/10/2007-10/11/2007 and in half-hour measurements on 10/17/2007 (Figures 5b and
376 7). Changes in EC flux associated with snowfall on 10/14/2007 were not possible to
377 assess due to gaps in the time series of EC flux. From 09/08/2006 to 10/24/2006, average
378 daily EC CO_2 flux was most strongly positively correlated with average daily
379 atmospheric pressure (correlation coefficient = 0.52) and inversely correlated with
380 average daily wind speed (correlation coefficient = -0.33) at one-day time lag (Figure 5a
381 and b). From 09/08/2006 to 09/22/2006 (zone I, Figure 5a and b), average daily EC CO_2
382 flux was more strongly correlated with average daily wind speed (correlation coefficient
383 = -0.70) than with average daily atmospheric pressure (correlation coefficient = 0.57).
384 However, from 09/24/2006 to 10/10/2006 (zone II, Figure 5a and b), EC CO_2 flux was
385 more strongly correlated with atmospheric pressure (correlation coefficient = 0.64) than
386 with wind speed (correlation coefficient = -0.39).
387

388 *4.6. Eddy covariance heat fluxes*

389

390 Measured *H* from 09/08/2006 to 10/24/2006 ranged from -91.9 to 466 W m^{-2}, with a
391 mean and standard deviation of 52.2 and 106.2 W m^{-2}, respectively. Measured *LE* ranged
392 from -99.9 to 176.4 W m^{-2}, with a mean and standard deviation of 19.3 and 34.7 W m^{-2},
393 respectively.

394

395 Neglecting the heat stored in the air beneath the sensors and horizontal advection, the
396 one-dimensional energy balance for the tree kill can be written as:

397

398 $$Rn - G = LE + H, \quad (3)$$

399

400 where *Rn* and *G* are the net radiation and heat flux into the soil, respectively. Their
401 difference represents the available energy. Figure 11 shows *LE* + *H* versus *Rn* – *G*
402 measured at the HLTK from 09/08/2006 to 10/24/2006. Data were categorized based on
403 time of day using PAR measurements and atmospheric stability using the stability
404 parameter ξ

405

406 $$\xi = \frac{z_m - d}{L} \quad (4)$$

407

408 (Garrat, 1992). *d* is the zero-plane displacement, estimated as 63% of canopy height,
409 which we assumed to equal zero based on absence of a canopy within the much of the
410 source areas. Measured turbulent heat fluxes were well correlated with available energy

411 (R^2 = 0.77 for 1:1 line). We calculated the relative difference between $H + LE$ and $Rn - G$, expressed as percent of $H + LE$. Systematic energy imbalances were observed,
413 depending on time of day and atmospheric stability. The mean relative difference for
414 energy fluxes measured at night was 44.1%. For fluxes measured during the day during
415 neutral and stable conditions ($\xi > -0.1$), the mean relative difference was -47.3%, whereas
416 it was -34.8% for fluxes measured during unstable-daytime ($\xi \leq -0.1$) periods. No
417 systematic relationships were observed between $\overline{w}$ and the relative difference between H
418 $+ LE$ and $Rn - G$.
419
420 **5. Discussion**
421
422 *5.1. Performance evaluation of eddy covariance*
423
424 The average CO_2 flux (1346 g m^{-2} d^{-1}) measured by EC from 09/08/2006 to 10/24/2006 at
425 the HLTK (Figure 7) fell within the range of average fluxes (691 to 1382 g m^{-2} d^{-1})
426 measured by Anderson and Farrar (2001) during their three sampling campaigns in 1996-
427 1998. While the general similarity of measured values is encouraging, direct comparison
428 of the two studies is not possible due to the different flux source areas that were sampled
429 in the two studies. For example, the EC stations in the Anderson and Farrar (2001) study
430 were located north of our EC station (Figure 2); thus, portions of asphalt parking lot were
431 likely located within their flux source areas. In addition, comparison of EC fluxes
432 measured in the different studies will also be complicated by the large spatial-temporal

433 variations in surface CO_2 fluxes that occur within the tree kill on diurnal to inter-annual
434 timescales (e.g., Gerlach et al., 1998; Rogie et al., 2001; Lewicki et al., 2007).
435
436 We used footprint modeling to compare EC to chamber measurements of CO_2 fluxes at
437 the HLTK. With a mean relative difference of –0.3 ± 2.7% between half-hour EC and
438 footprint CO_2 fluxes (Figure 9), the measurements were on average nearly unbiased. At
439 relatively high flux, half-hour EC CO_2 fluxes tended to be biased high, relative to
440 footprint CO_2 fluxes. Also, datasets for the HLTK were moderately correlated (Figure
441 10a), with a variance in the relative difference of 23%. Table 2 shows relative
442 differences between EC and chamber CO_2 fluxes in volcanic and hydrothermal systems.
443 Using footprint models to compare chamber to EC CO_2 fluxes, the Werner et al. (2000;
444 2003) investigations are most analogous to this study. Our results for the HLTK were
445 similar to those reported by Werner et al. (2003) for diffusely degassing areas of
446 Solfatara volcano, Italy (Figure 10a; Table 2). On average, a larger relative difference
447 was observed between EC and chamber CO_2 fluxes for the Yellowstone National Park
448 data, likely due in part to the presence of hydrothermal features within the EC source
449 areas (Werner et al., 2000). Also, a larger dataset would be required for Yellowstone for
450 closer comparison with other studies. While Anderson and Farrar (2001) did not directly
451 compare EC to chamber CO_2 fluxes at the HLTK based on footprint modeling, they
452 reported relative differences between average EC CO_2 fluxes calculated for the duration
453 of their pilot studies and average chamber CO_2 fluxes measured in independent studies.
454 Based on this analysis, they reported significantly larger negative bias in EC relative to
455 chamber flux measurements than reported in other studies (Table 2).

Several factors may account for the differences observed between half-hour EC and footprint CO_2 fluxes (Figures 9 and 10a). First, both the EC method and the analytic footprint model assume homogeneous surface fluxes, flat terrain, and uniform surface roughness. However, systematic errors associated with violations to these assumptions could be difficult to diagnose because they will depend on interactions between terrain, wind direction and speed, and atmospheric stability. EC fluxes were on average unbiased relative to footprint fluxes and no systematic relationship was observed when comparing the relative difference between the EC and footprint CO_2 fluxes and the ranges of L, u_*, time of day, or wind direction considered in the analysis. However, we observed positive bias of EC relative to footprint CO_2 fluxes at relatively high flux. Also, the relative difference between EC and footprint CO_2 fluxes increased as $\overline{w}$ became more negative. Non-zero $\overline{w}$ values can be indicative of advective flux (e.g., Lee, 1998; Turnipseed et al., 2003), but interpretations of their effect on EC fluxes vary. Lee (1998) suggested that horizontal flow divergence below the EC measurement height caused negative $\overline{w}$ and loss of CO_2 flux at night under stable conditions over a deciduous forest. However, over a coniferous forest in mountainous terrain, Turnipseed et al. (2003) interpreted positive $\overline{w}$ values and loss of CO_2 flux at night under stable stratification to reflect flow convergence near the EC tower due to local changes in terrain. We only deployed a single EC station, and so we cannot assess the horizontal advective fluxes necessary to close the conservation of mass equations that would be required to understand the sign and cause of the bias we observe. We suspect that the negative bias in $\overline{w}$ and positive bias in EC CO_2 flux at high flux we observe under unstable conditions

479 likely result from air flow changes as wind interacts with the complicated terrain of the
480 study area. Presumably, a planar-fit coordinate rotation (Wilczak et al., 2001) could be
481 used to reduce vertical-wind bias. Finally, the effects of wind drag on downhill
482 horizontal flows would likely only subtly affect wind speed gradients, since standing
483 dead wood within the EC source areas was sparsely distributed and free of foliage and
484 fine branches. In fact, the observed negative bias in $\overline{w}$ is opposite to what we might
485 expect if wind drag slowed airflow and forced up-flow near the EC station.
486
487 Second, aspects of the chamber method can lead to underestimation or overestimation of
488 soil CO_2 fluxes. For example, fluxes measured by vented chambers can be systematically
489 high during windy times due to Venturi effects (e.g., Conen and Smith, 1998). While we
490 cannot rule this effect out for all measurements, we did not find evidence for systematic
491 overestimation of chamber CO_2 fluxes at the HLTK. In addition, some infiltration of
492 atmospheric air into the chamber during windy periods could have occurred, biasing
493 chamber CO_2 fluxes low. However, this effect would not account for the spatially
494 systematic decrease in soil CO_2 flux that was observed on 09/14/2007 with high average
495 daily wind speed, and then following the passage of the cold front on 09/16/2007 when
496 low average daily wind speed was observed (Figure 6; Lewicki et al., 2007). Rather, we
497 would expect wind-driven air infiltration into the chamber to affect chamber flux
498 measurements randomly over the study area. Placement of the chamber on the soil
499 surface disturbs the soil properties and gas flow during the time of measurement, which
500 can lead to systematically low flux measurements when advective soil gas flow occurs
501 (Welles et al., 2000; Evans et al., 2001). While we attempted to correct chamber

measurements for this effect prior to the footprint analysis, it is possible that chamber fluxes were under-corrected at relatively high flux, thus potentially contributing to the high EC relative to footprint CO_2 fluxes.

Third, we demonstrated that large variations occur in the spatial distribution and magnitude of surface CO_2 fluxes over relatively short periods of time within the tree kill area (Figure 6), which are difficult to characterize with the chamber method, even when measurements are repeated on a daily basis. As a result, our assumption that on any given day, over the entire day, the distribution of source CO_2 fluxes is equal to the measured chamber fluxes on that day probably introduced error into the comparison. Finally, random errors associated with both the EC and chamber methods (e.g., Chiodini et al., 1998; Baldocchi, 2003) were likely important sources of variability in the comparison. Nonetheless, given all of the complexities of the HLTK site, it is encouraging that relatively small biases exist in our dataset, which reinforces our assertion that the EC method may be used with some success in such environments.

When the half-hour EC and footprint CO_2 fluxes were averaged over daily timescales, the correlation improved substantially (Figure 10b). Also, the positive bias observed at relatively high flux in half-hour EC relative to footprint CO_2 fluxes was reduced in the average daily fluxes. Since each grid of chamber measurements was typically completed over ~8 hours on a given day, averaging EC and footprint CO_2 fluxes over day-long periods allowed us to evaluate the measurements over more comparable timescales. This likely contributed to the improved correlation observed between average daily EC and

525 footprint CO_2 fluxes. Our results suggest that if monitoring variations in surface CO_2
526 fluxes over timescales longer than a day is adequate for the investigation of interest (e.g.,
527 volcano monitoring), then the EC technique can perform well under certain complex site
528 conditions.
529
530 Average *H* and *LE* values measured from 09/08/2006 to 10/24/2006 fell within the range
531 of average values measured by Anderson and Farrar (2001) during their three sampling
532 campaigns at the HLTK. These values were lower than those measured by Werner et al.
533 (2006) at Solfatara volcano, which is expected due to the relatively high soil temperatures
534 and steam condensation in soils in the Solfatara hydrothermal area. Also, Werner et al.
535 (2006) found that measurements of *H* and *LE* were positively correlated with EC CO_2
536 fluxes in the Solfatara hydrothermal area, reflecting a large volcanic component in all
537 fluxes. We found no systematic relationship between these parameters at the HLTK, due
538 to the different sources of heat (non-volcanic) and CO_2 (volcanic).
539
540 We further assessed the performance of EC at the HLTK by comparing EC heat flux
541 measurements to measurements made by independent methods. While the degree of
542 energy balance closure obtained in the field is directly applicable to evaluation of *H* and
543 *LE*, its utility in the evaluation of CO_2 fluxes will depend on whether sources of error are
544 associated with the EC method or in determining the available energy terms (e.g., Wilson
545 et al., 2002). The degree of energy balance closure observed (Figure 11) fell within the
546 range of that observed at FLUXNET sites, where energy fluxes were measured over a
547 wide range of ecosystems and climates, typically with more ideal terrain and surface flux

548 characteristics than observed at the HLTK (Wilson et al., 2002). Turbulent heat fluxes at
549 the tree kill were typically underestimated relative to available energy during daytime
550 hours, whereas during nighttime hours, turbulent heat fluxes were overestimated relative
551 to available energy.
552
553 Lack of complete energy balance closure can result from a range of issues, including
554 systematic and random sampling errors, lack of complete estimation of heat stored
555 beneath the EC sensors, inherent low and high pass filtering associated with the EC
556 method, and advection of heat induced by horizontal heterogeneity of surface fluxes and
557 complex terrain (e.g., Wilson et al., 2002). While it is not possible to unequivocally
558 determine the sources of error and their relative importance in the energy balance
559 assessment, one or more issues could be relevant to the HLTK area. First, the source
560 areas sampled by the soil heat flux plates (cm^2 scale), net radiometer (m^2 scale), and EC
561 vary between one another by up to several orders of magnitude. Therefore, variations in
562 the surface conditions (e.g., slope geometry and sun facing angle, presence of rocks and
563 standing/fallen deadwood) and climate within the different source areas likely induced
564 systematic biases in the energy balance calculation. Second, while the poorer energy
565 balance closure observed during neutral-and-stable-daytime relative to unstable-daytime
566 periods could be due in part to heat storage in the air beneath the EC sensors, this effect
567 was unlikely to be substantial because of the short height of the EC system and either
568 near-absence of a canopy in the EC system source areas. Third, advection associated
569 with wind speed gradients could, in principal, bias EC heat fluxes similarly to CO_2.
570 Since we observed (1) no systematic relationship between $\overline{w}$ and the relative difference

between $H + LE$ and $Rn - G$ and (2) substantially greater bias in EC heat flux versus available energy measurements than in EC versus footprint CO_2 fluxes, it is likely that the role of advection is minor relative to other factors such as difference in source area in the lack of energy balance closure at the HLTK.

5.2. Influence of meteorological forcing on surface CO_2 fluxes

Lewicki et al. (2007) showed that large spatio-temporal variations in surface CO_2 fluxes measured by the chamber method at the HLTK from 09/12/2006 to 09/21/2006 were meteorologically driven. They calculated total CO_2 discharge rates for the study area based on chamber measurements and found them to be positively correlated with average daily atmospheric pressure and inversely correlated with average daily wind speed, most strongly at one-day time lag. While the processes driving these relationships likely involved complex interactions between meteorology, topography, and vadose zone gas flow, Lewicki et al. (2007) suggested that spatio-temporal changes in surface CO_2 fluxes may have been primarily due to dynamic coupling between the flow of volcanic CO_2 at depth within the vadose zone and wind.

Despite the complications introduced into the EC CO_2 flux time series by the temporally varying flux source area, we observed similar relationships between average daily EC CO_2 fluxes and average daily wind speed and atmospheric pressure from 09/08/2006 to 09/22/2006 (zone I, Figure 5a and b) to those observed by Lewicki et al. (2007) for chamber measurements over a similar time period. The relatively high degree of

correlation observed between average daily EC CO_2 flux and wind speed from 09/08/2006 to 09/22/2006 was likely due to the cold front that passed through the region during that time bringing high winds that could have modulated vadose zone gas flow (Lewicki et al., 2007). However, from 09/24/2006 to 10/10/2006 (zone II, Figure 5), EC CO_2 flux was more strongly correlated with atmospheric pressure and more weakly correlated with wind speed. This was probably due to the lower magnitude variations in average daily wind speed over this time period having less influence on subsurface gas flow to the atmosphere. Overall, our results indicate that similar to the chamber method, EC can be used to monitor background changes in volcanic CO_2 fluxes driven by meteorological forcing, and presumably changes related to deeply derived processes such as volcanic activity.

It is likely that precipitation events, and associated increases in soil moisture content also affected surface CO_2 fluxes at the HLTK. However, it was only possible to assess the relationship between EC CO_2 fluxes and precipitation in a limited fashion due to gaps in the time series of EC flux caused by data filtering for wind direction, u_*, and stationarity. This emphasizes the issue that potentially large gaps in time series of EC flux data must be tolerated, particularly at a site such as the HLTK. For example, we lost about half of the half-hour EC CO_2 flux data for the given wind direction range of interest (190 to 360^o) due to insufficient turbulence and non-stationarity in the data. Automated and continuous chamber measurements at a fixed location within the study area (e.g., Rogie et al., 2001; Werner et al., 2003) would be valuable to supplement EC data.

6. Summary and Conclusions

We measured a six-week time series of EC CO_2 and heat fluxes at the HLTK on Mammoth Mountain, a site with heterogeneous distribution of source fluxes and complex terrain that challenged the underlying assumptions of EC theory.

1. Half-hour EC CO_2 fluxes were compared with chamber fluxes measured repeatedly on a daily basis using footprint modeling. EC CO_2 fluxes were moderately correlated with, and on average unbiased relative to, footprint CO_2 fluxes. The average relative difference between HLTK EC and footprint CO_2 fluxes was similar to that reported for diffusely degassing areas at Solfatara volcano, Italy (Werner et al., 2003). Even though HLTK chamber CO_2 fluxes were measured on a daily basis, it was not possible to completely characterize spatio-temporal variations in source CO_2 fluxes on the time scale of the EC measurements. This factor, as well as advection of CO_2 due to topographic variations and the inherent random errors associated with both the EC and chamber methods likely contributed to the differences observed between CO_2 fluxes measured by the two techniques.

2. Average daily EC CO_2 fluxes were well correlated with average daily footprint CO_2 fluxes, indicating that when random error is reduced in CO_2 flux measurements by temporal averaging, the EC technique can perform well under certain complex site conditions. However, potential volcanic and geothermal sites for deployment of EC must be evaluated on an individual basis to assess viability of the method.

3. Turbulent heat fluxes were well correlated with available energy at the HLTK and the degree of energy balance closure fell within the range observed in many investigations conducted in contrasting ecosystems and climates with more ideal terrain and surface flux characteristics.

4. Average daily EC CO_2 fluxes were correlated with both average daily wind speed and atmospheric pressure over the observation period, the degree to which depended on the magnitude of the fluctuations in the atmospheric parameters. The relationships between EC CO_2 fluxes and wind speed and atmospheric pressure were similar to those observed between chamber CO_2 fluxes and the atmospheric parameters over a comparable time period. Similar to the chamber method, EC can be used to monitor background changes in volcanic CO_2 fluxes driven by meteorological forcing, and presumably changes related to deeply derived processes such as volcanic activity.

5. EC provides the benefit over the chamber method of a time and space-averaged measurement of surface CO_2 flux that is essentially fully automated. However, potentially large gaps in time series of data must be tolerated with EC, depending on site characteristics and atmospheric conditions. Also, the spatial distribution of surface CO_2 fluxes cannot be mapped in detail by EC, as it can by the chamber method. The chamber and EC methods are therefore best used together, providing complementary information in volcanic gas surveillance programs.

Acknowledgements

We thank C. Werner, an anonymous reviewer, and S. Biraud for comments that greatly improved the manuscript, T. Tosha and R. Aoyagi for assistance in the field, and H.P. Schmidt for the FSAM source code. This work was supported by the Ministry of Economy, Trade, and Industry (METI) of Japan through the Lawrence Berkeley National Laboratory Sponsored Project Office Contract No. LB06002281, and by the Zero Emissions Research and Technology (ZERT) project, supported by the Assistant Secretary for Fossil Energy, Office of Sequestration, Hydrogen, and Clean Coal Fuels, through the National Energy Technology Laboratory, U.S. Department of Energy, under Contract No. DE-AC02-05CH11231.

675 **References**

676 Anderson, D.E., Farrar, C.D., 2001. Eddy covariance measurement of CO_2 flux to the
677 atmosphere from an area of high volcanogenic emissions, Mammoth Mountain,
678 California. Chemical Geology, 177, 31–42.

679 Aubinet, M., Grelle, A., Ibrom, A., et al., 2000. Estimates of the annual net carbon and
680 water exchange of European forests: the EUROFLUX methodology. Advances in
681 Ecological Research, 30, 113–175.

682 Bailey, R.A., 1989. Geologic map of the Long Valley Caldera, Mono-Inyo Craters
683 volcanic chain and vicinity, eastern California, scale 1:62,500. U.S. Geological
684 Survey Miscellaneous Investigations Map, I–1933.

685 Baldocchi, D.D., 2003. Assessing the eddy covariance technique for evaluating carbon
686 dioxide exchange rates of ecosystems: past, present, and future. Global Change
687 Biology, 9, 479–492.

688 Baldocchi, D.D., Hicks, B.B., Meyers, T.P., 1988. Measuring biosphere-atmosphere
689 exchanges of biologically related gases with micrometeorological methods.
690 Ecology, 69, 1331–1340.

691 Baubron, J.-C., Allard, P., Sabroux, J.-C., Tedesco, D., Toutaln, J.P., 1991. Soil gas
692 emanations as precursory indicators of volcanic eruptions. Journal of the
693 Geological Society, 148, 571–576.

694 Bergfeld, D., Goff, F., Janik, C.J., 2001. Elevated carbon dioxide flux at the Dixie Valley
695 geothermal field, Nevada; relations between surface phenomena and the
696 geothermal reservoir. Chemical Geology, 177, 43–66.

Billesbach, D.P., Fischer, M.L., Torn, M.S., Berry, J.A., 2004. A portable eddy covariance system for the measurement of ecosystem-atmosphere exchange of CO_2, water vapor, and energy. Journal of Atmospheric and Oceanic Technology 21, 639–650.

Chiodini, G., Cioni, G. R., Guidi, M., Raco, B., Marini, L., 1998. Soil CO_2 flux measurements in volcanic and geothermal areas. Applied Geochemistry, 13, 543–552.

Conen, F., Smith, K.A., 1998. A re-examination of closed flux chamber methods for the measurement of trace gas emissions from soils to the atmosphere. European Journal of Soil Science, 49, 701-707.

Connor, C.B., Clement, B.M., Song, X.D., Lane, S.B., Westthomas, K., 1993. Continuous monitoring of high-temperature fumaroles on an active lava dome, Volcan Colima, Mexico- Evidence of mass-flow variation in response to atmospheric forcing. Journal of Geophysical Research, 98, 19,713–19,722.

Evans, W. C., Sorey, M. L., Kennedy, B. M., Stonestrom, D. A., Rogie, J. D., Shuster, D.L., 2001. High CO_2 emissions through porous media: Transport mechanisms and implications for flux measurement and fractionation. Chemical Geology, 177, 15–29.

Farrar, C.D., Sorey, M.L., Evans, W.C., Howle, J.F., Kerr, B.D., Kennedy, B.M., King, Y., Southon, J.R., 1995. Forest-killing diffuse CO_2 emission at Mammoth Mountain as a sign of magmatic unrest. Nature, 376, 675–678.

718 Farrar, C.D., Neil, J.M., Howle, J.F., 1998. Magmatic carbon dioxide emissions at
719 Mammoth Mountain, California. U.S. Geological Survey Water Resources
720 Investigation Report 98–4217, 34 pp.
721 Folken, Th., Wichura, B., 1996. Tools for quality assessment of surface-based flux
722 measurements. Agricultural and Forest Meteorology, 78, 83–105.
723 Garrat, 1992. The Atmospheric Boundary Layer. Cambridge University Press,
724 Cambridge, 316 p.
725 Gerlach, T.M., Doukas, M.P., McGee, K.A., Kessler, R., 1998. Three-year decline of
726 magmatic CO_2 emissions from soils of a Mammoth Mountain tree kill: Horseshoe
727 Lake, CA, 1995-1997. Geophysical Research Letters, 25, 1947–1950.
728 Gerlach, T.M., Doukas, M.P., McGee, K.A., Kessler, R., 2001. Soil efflux and total
729 emission rates of magmatic CO_2 at the Horseshoe Lake tree kill, Mammoth
730 Mountain, California, 1995-1999. Chemical Geology, 177, 101–116.
731 Granieri, D., Chiodini, G., Marzocchi, W., Avino, R., 2003. Continuous monitoring of
732 CO_2 soil diffuse degassing at Phlegrean Fields (Italy): influence of environmental
733 and volcanic parameters. Earth and Planetary Science Letters, 212, 167–179.
734 Hernandez, P.A., Perez, N., Salazar, J.M., Nakai, S., Notsu, K., Wakita, H., 1998.
735 Diffuse emissions of carbon dioxide, methane, and helium-3 from Teide volcano,
736 Tenerife, Canary Islands. Geophysical Research Letters, 25, 3311–3314.
737 Hernandez, P.A., Notsu, K., Salazar, J.M., Mori, T., Natale, G., Okada, H., Virgilli, G.,
738 Shimoike, Y., Sato, M., Perez, N.M., 2001. Carbon dioxide degassing by
739 advective flow from Usu volcano, Japan. Science, 2001, 83–86.

740 Hill, D.P., 1996. Earthquakes and carbon dioxide beneath Mammoth Mountain,
741 California. Seismological Research Letters, 67, 8–15.
742 Hill, D.P., Prejean, S.G., 2005. Volcanic unrest beneath Mammoth Mountain, California.
743 Journal of Volcanology and Geothermal Research, 146, 257–283.
744 Horst, T.W., Weil, J.C., 1992. Footprint estimation for scalar flux measurements in the
745 atmospheric surface-layer. Boundary-Layer Meteorology, 59, 279-296.
746 Kaimal, J.C., Finnigan, J.J., 1994. Atmospheric Boundary Layer Flows: Their Structure
747 and Measurement. Oxford University Press, Oxford.
748 Klusman, R.W., Moore, J.N., LeRoy, M.P., 2000. Potential for surface gas
749 measurements in exploration and surface evaluation of geothermal resources.
750 Geothermics, 29, 637–670.
751 Lee, X., 1998. On micrometeorological observations of surface-air exchange above tall
752 vegetation. Agricultural and Forest Meteorology, 91, 39-49.
753 Lewicki, J.L., Bergfeld, D., Cardellini, C., Chiodini, G., Granieri, D., Varley, Werner, C.,
754 2005. Comparative soil CO_2 flux measurements and geostatistical estimation
755 methods on Masaya volcano. Nicaragua, Bulletin of Volcanology, 68, 76-90, doi:
756 10.1007/s00445-005-0423-9.
757 Lewicki, J.L., Hilley, G.E., Tosha, T., Aoyagi, R., Yamamoto, K., Benson, S.M., 2007.
758 Dynamic coupling of volcanic CO_2 flow and wind at the Horseshoe Lake tree kill,
759 Mammoth Mountain, California. Geophysical Research Letters, 34, L03401,
760 doi:10.1029/2006GL028848.

McGee, K.A., Gerlach, T.M., 1998. Annual cycle of magmatic CO_2 in a tree-kill soil at Mammoth Mountain, California: Implications for soil acidification. Geology, 26, 463–466.

McGee, K.A., Gerlach, T.M., Kessler, R., Doukas, M.P., 2000. Geochemical evidence for a magmatic CO_2 degassing event at Mammoth Mountain, California, September-December 1997. Journal of Geophysical Research, 105, 8447–8456.

Rahn, T.A., Fessenden, J.E., Wahlen, M., 1996. Flux chamber measurements of anomalous CO_2 emission from the flanks of Mammoth Mountain, California. Geophysical Research Letters, 23, 1861–1864.

Rogie, J.D., Kerrick, D.M., Sorey, M.L., Chiodini, G., Galloway, D.L., 2001. Dynamics of carbon dioxide emission at Mammoth Mountain, California. Earth and Planetary Science Letters, 188, 535–541.

Schmid, H.P., 1997. Experimental design for flux measurements: matching scales of observations and fluxes. Agricultural and Forest Meteorology, 87, 179–200.

Turnipseed, A.A., Anderson, D.E., Blanken, P.D., Baugh, W.M., Monson, R.K., 2003. Airflows and turbulent flux measurements in mountainous terrain Part 1. Canopy and local effects. Agricultural and Forest Meteorology, 119, 1–21.

Turnipseed, A.A., Anderson, D.E., Burns, S., Blanken, P.D., Monson, R.K., 2004. Airflows and turbulent flux measurements in mountainous terrain Part 2. Mesoscale effects. Agricultural and Forest Meteorology, 125, 187–205.

Webb, E.K., Pearman, G.I., Leuning, R., 1980. Correction of flux measurements for density effects due to heat and water vapour transfer, Quarterly Journal of Royal Meteorological Society, 106, 85–100.

784 Welles, J.M., Demetriades-Shah, T.H., McDermitt, D.K., 2000. Considerations for
785 measuring ground CO_2 effluxes with chambers. Chemical Geology, 177, 3-13.
786 Werner, C., Cardellini, C., 2006. Comparison of carbon dioxide emissions with fluid
787 upflow, chemistry, and geologic structures at the Rotorua geothermal system,
788 New Zealand. Geothermics, 35, 221–238.
789 Werner, C., Wyngaard, J.C., Brantley, S.L., 2000. Eddy-correlation measurement of
790 hydrothermal gases. Geophysical Research Letters, 27, 2925–2928.
791 Werner, C., Chiodini, G., Voigt, D., Caliro, S., Avino, R., Russo, M., Brombach, T.,
792 Wyngaard, J., Brantley, S., 2003. Monitoring volcanic hazard using eddy
793 covariance at Solfatara volcano, Naples, Italy. Earth and Planetary Science
794 Letters, 210, 561–577.
795 Werner, C., Chiodini, G., Granieri, D., Caliro, S., Avino, R., Russo, M., 2006. Eddy
796 covariance measurements of hydrothermal heat flux at Solfatara volcano, Italy.
797 Earth and Planetary Science Letters, 244, 72–82.
798 Wilczak, J.M., Oncley, S.P., Stage, S.A., 2001. Sonic anemometer tilt correction
799 algorithms. Boundary Layer Meteorology, 99, 127-150.
800 Wilson, K., Goldstein, A., Falge, E., Aubinet, M., Baldocchi, D., Berbigier, P.,
801 Bernhofer, C., Ceulemans, R., Dolman, H., Field, C., Grelle, A., Ibrom, A., Law,
802 B.E., Kowalski, A., Meyers, T., Moncrieff, J., Monson, R., Oechel, W.,
803 Tenhunen, J., Valentini, R., Verma, S., 2002. Energy balance closure at
804 FLUXNET sites. Agricultural and Forest Meteorology, 113, 223–243.
805

Figure Captions

Figure 1. View of the Horseshoe Lake tree kill located on the southeastern flank of Mammoth Mountain, adjacent to Horseshoe Lake. Red square shows approximate location of EC station.

Figure 2. Digital elevation model of the HLTK study area, outlined by white line (modified from Lewicki et al., 2007). White dots show locations of the chamber CO_2 flux measurement points. Red and yellow squares show approximate locations of EC stations in the present and Anderson and Farrar (2001) studies, respectively.

Figure 3. Plot of EC CO_2 flux versus friction velocity (u_*). Solid line is running average of EC CO_2 flux over a 0.1 m s^{-1} u_* window. Vertical dashed line shows $u_* = 0.25$ m s^{-1}.

Figure 4. Wind rose showing joint frequency distribution of mean horizontal wind speed and direction (half-hour averages) from 09/08/2006 to 10/24/2006, constructed using Frequency Works.

Figure 5. (a) Time series of average daily atmospheric pressure (stars) and wind speed (dots). (b) Time series of average daily EC CO_2 flux corresponding to wind directions from 250 to 290^o. Symbols indicate number of measurements (n) used to calculate average daily EC CO_2 fluxes. Error bars are standard error of mean. Average daily EC CO_2 fluxes are missing on days where filtering has entirely eliminated half-hour data. Diamonds are average of chamber CO_2 fluxes measured repeatedly on daily basis over entire grid area grid from 09/12/2006 to

09/21/2006. Dark gray zones in indicate approximate timing of precipitation events. See text for explanations of light grayed zones I and II.

Figure 6 (a-i). Time series (09/12/2006 to 09/21/2006) of maps of log chamber CO_2 flux. White squares denote approximate location of EC station.

Figure 7. Time series of EC CO_2 flux corresponding to mean wind direction between 190 and 360°, $u_* > 0.25$ m s^{-1}, and stationary measurements. Gray zones indicate approximate timing of precipitation events.

Figure 8. Source areas (area within which 90% of the measured EC flux was derived from) for 73 modeled footprints. Square shows location of EC station.

Figure 9. Histogram of the relative difference between EC and footprint CO_2 fluxes, expressed as percent of EC flux.

Figure 10. Plots of (a) EC CO_2 flux versus footprint CO_2 flux for half-hour EC measurements and (b) average daily EC CO_2 flux versus average daily footprint CO_2 flux. Error bars show standard error of mean. Gray area encompasses data from diffusely degassing areas at Solfatara volcano, Italy (Location 1; Werner et al., 2003).

Figure 11. Plot of sum of latent (*LE*) and sensible (*H*) heat flux measured by EC versus difference between net radiation (*Rn*) and soil heat flux (*G*) measured by radiometer and heat flux plates, respectively from 09/12/2006 to 09/21/2006. Red dots are measurements made during the nighttime. Black dots and squares are measurements made during neutral-and-stable-daytime ($\xi > -0.1$) and unstable-daytime ($\xi \leq -0.1$) periods. 1:1 line is shown.

852 Table 1. Daily averages of half-hour data used for EC-footprint CO_2 flux comparisons

853 and mean vertical wind speed.

Date	*n*	EC CO_2 flux ($g\ m^{-2}\ d^{-1}$)	Footprint CO_2 flux ($g\ m^{-2}\ d^{-1}$)	*L* (m)	u_* ($m\ s^{-1}$)	σ_v ($m\ s^{-1}$)	Wind dir. (^{o})	$\overline{w}$ ($m\ s^{-1}$)
09/12/2006	3	1437.3	1327.9	-63.7	0.32	1.4	263	-0.05
09/13/2006	5	1252.2	1134.5	-62.5	0.32	1.4	225	$0.03e^{-1}$
09/14/2006	23	856.8	1006.0	-1415.3	0.88	3.0	263	-0.26
09/18/2006	7	1032.4	1163.1	-76.9	0.37	1.5	236	-0.06
09/19/2006	14	1059.3	1061.4	-491.2	0.82	2.7	265	-0.25
09/20/2006	7	964.1	1060.5	-40.2	0.32	1.6	268	-0.09
09/21/2006	14	1436.4	1425.2	-60.4	0.51	1.9	262	-0.13

854

855 Table 2. Relative differences for EC and chamber CO_2 flux comparisons in volcanic and

856 hydrothermal systems.

Site	Mean ± standard deviation relative difference between EC and chamber CO_2 fluxes	n	Reference
Yellowstone National Park, USA	-4.1 ± 68 %	6	Werner et al. (2000)
Solfatara volcano, Italy	-0.4 ± 32%	66	Werner et al. (2003)
Mammoth Mountain, USA	-19 to -40 %	2	Anderson and Farrar (2001)
Mammoth Mountain, USA	-0.3 ± 23%	73	Present study

857 For Werner et al. (2000; 2003) and the present study, the relative difference is defined as

858 the half-hour EC CO_2 flux minus footprint CO_2 flux, expressed as per-cent EC CO_2 flux.

The mean and standard deviation of these values are reported. For Anderson and Farrar (2001), the relative difference is the mean EC CO_2 flux for study duration (two pilot studies were considered) minus the mean chamber CO_2 flux measured in independent studies, expressed as per-cent mean EC CO_2 flux. Only the range of these values is reported.

Figures.

Figure 1.

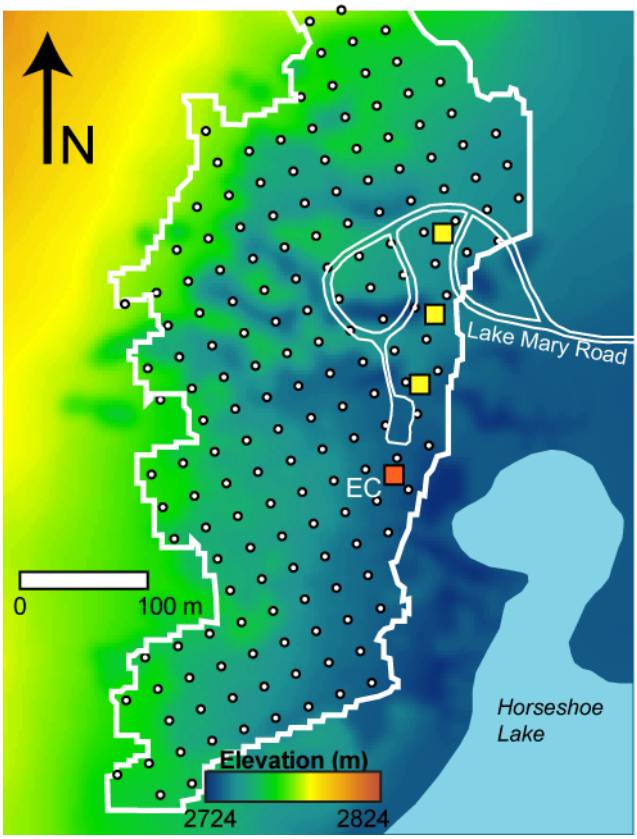

Figure 2.

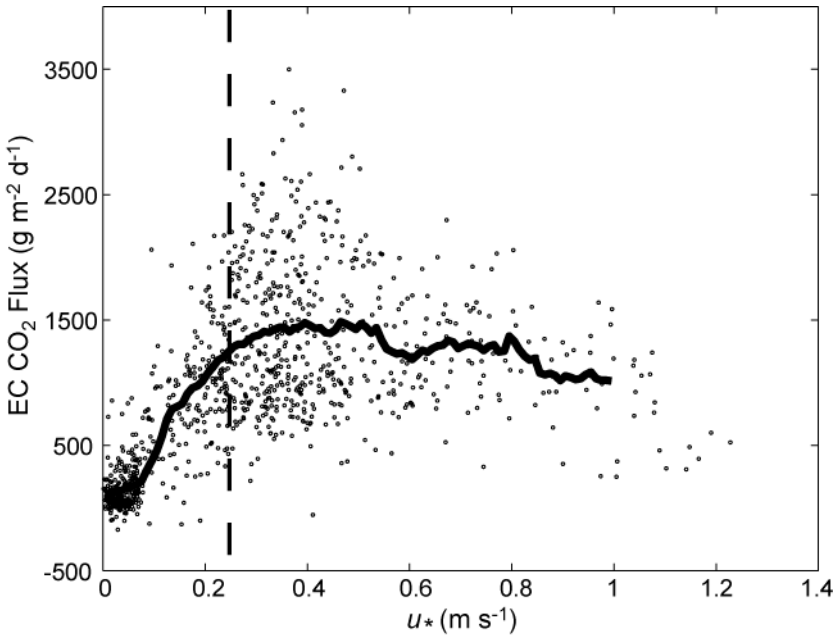

Figure 3.

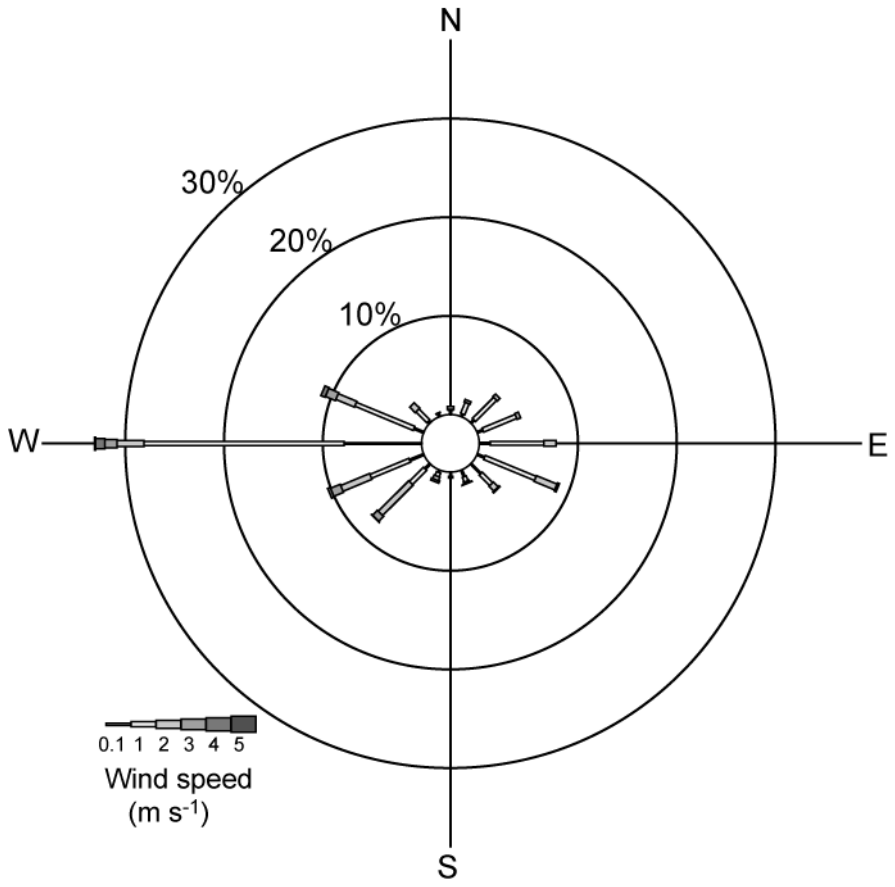

Figure 4.

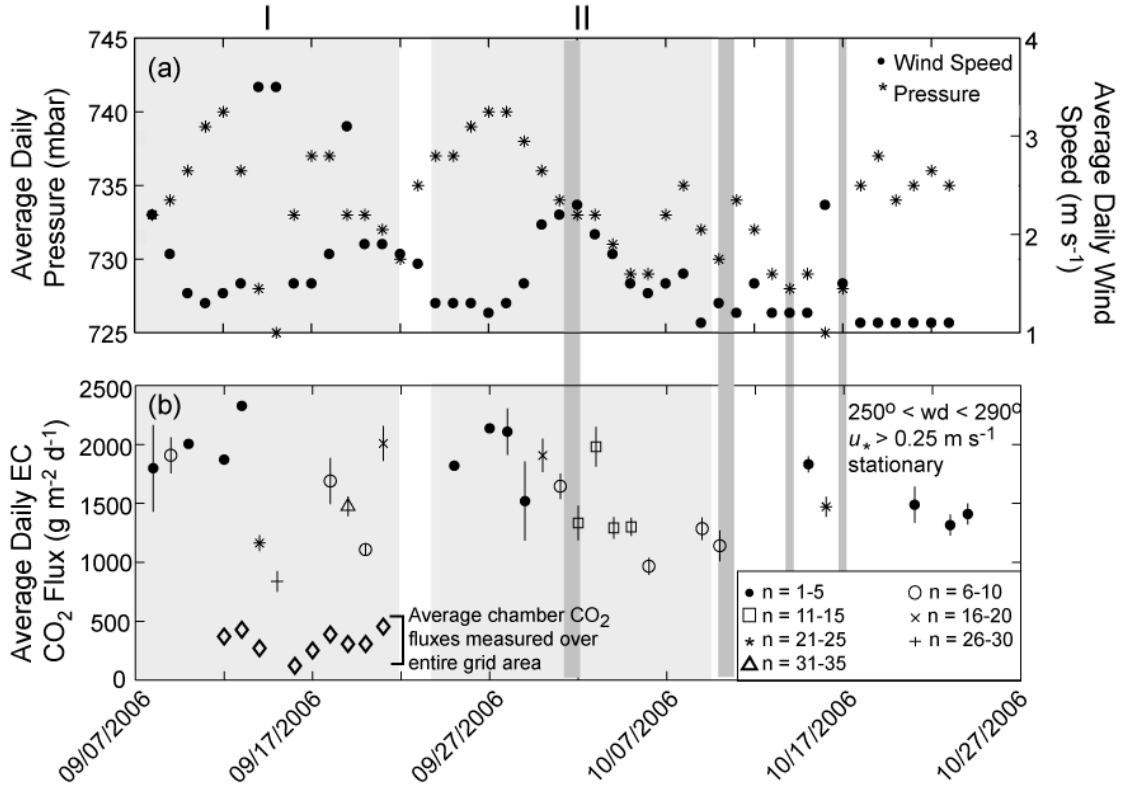

877
878
879 Figure 5.
880

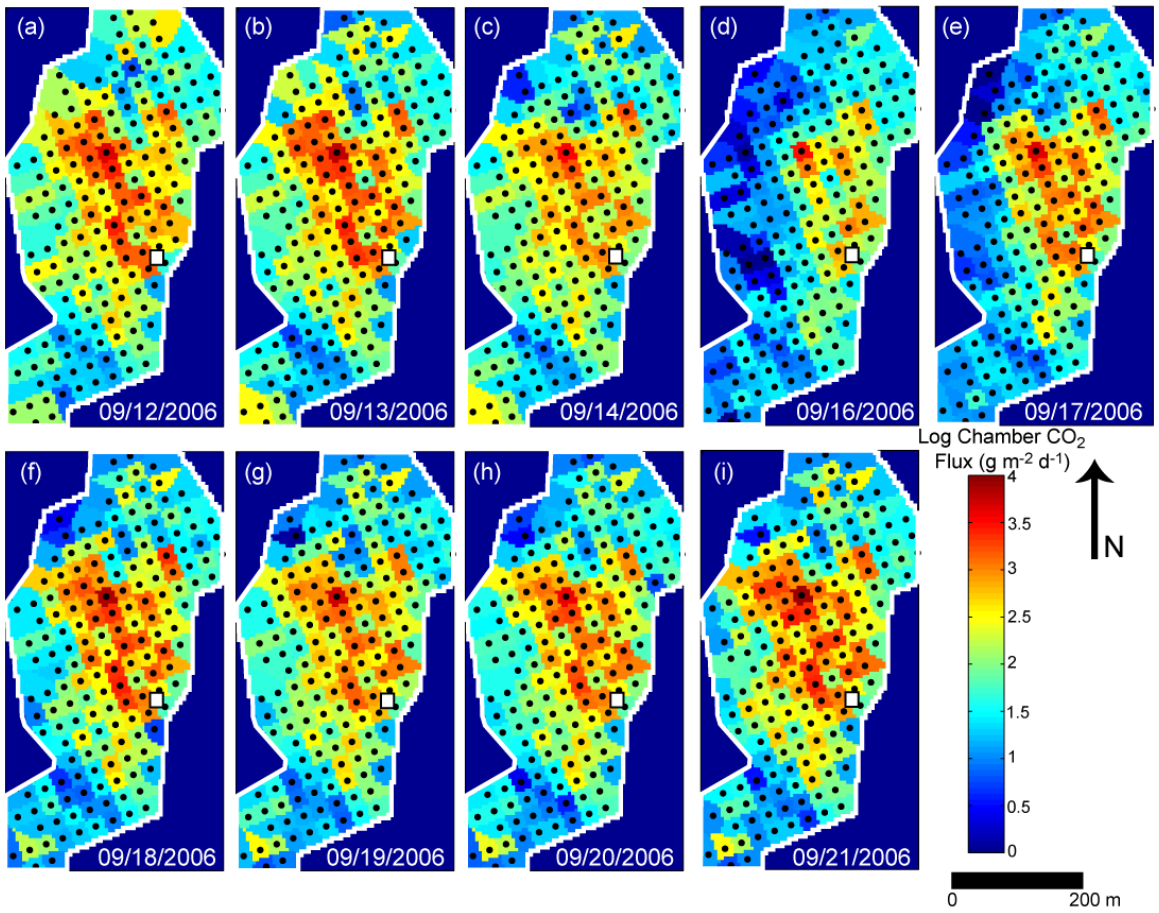

Figure 6.

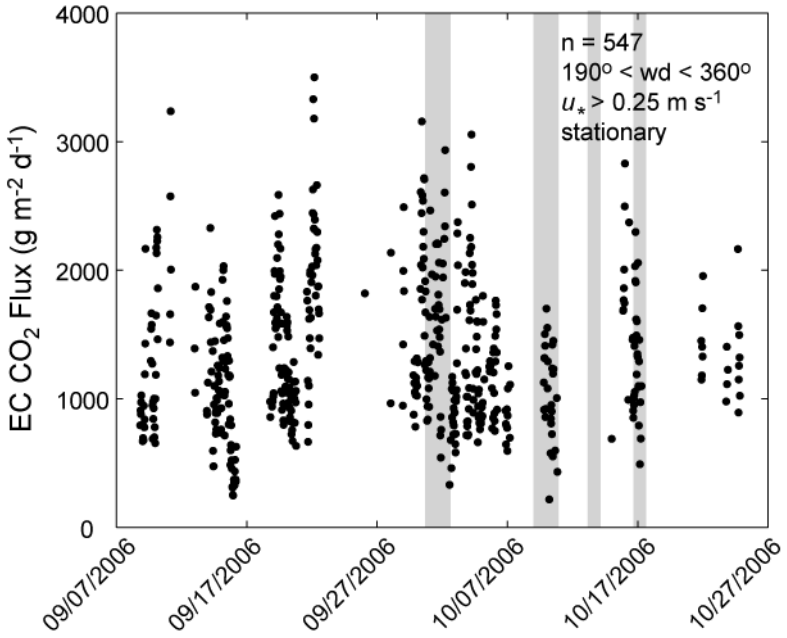

Figure 7.

887

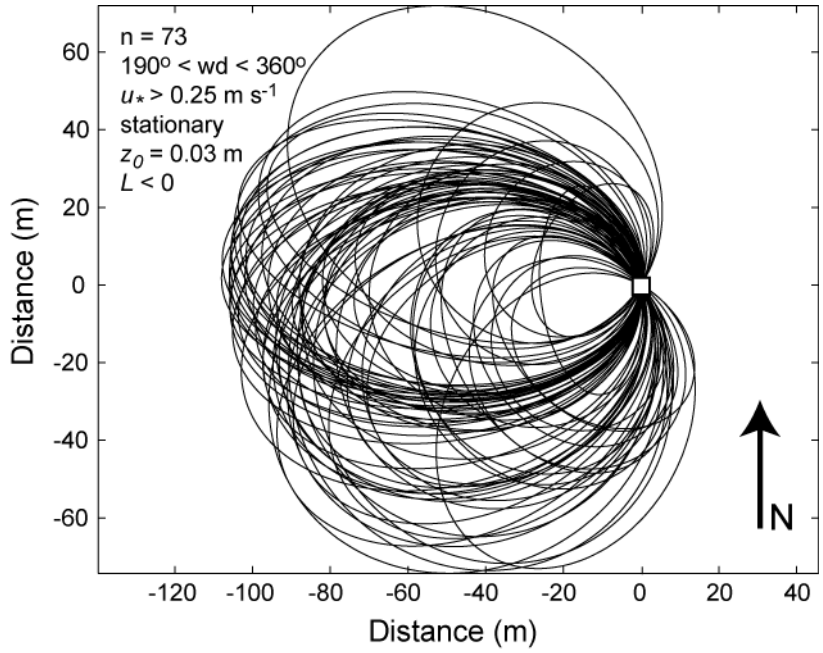

888
889 Figure 8.
890

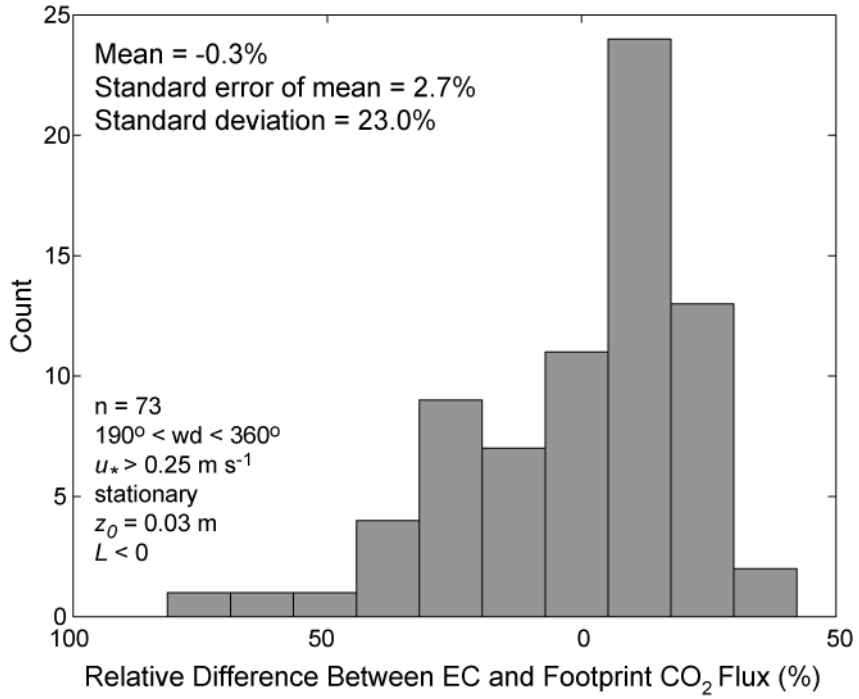

891
892 Figure 9.
893

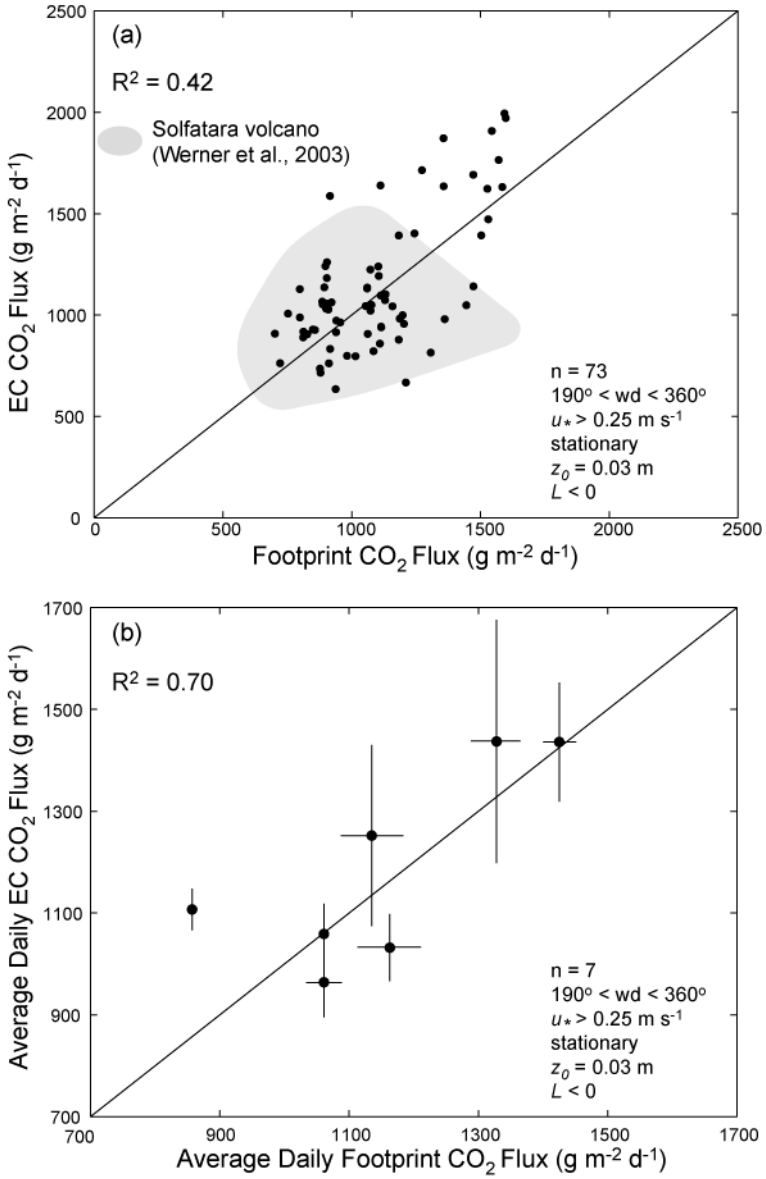
(a)
R² = 0.42
Solfatara volcano
(Werner et al., 2003)
n = 73
190° < wd < 360°
u* > 0.25 m s-1
stationary
z0 = 0.03 m
L < 0
EC CO2 Flux (g m-2 d-1)
Footprint CO2 Flux (g m-2 d-1)
0
500
1000
1500
2000
2500
(b)
R² = 0.70
n = 7
190° < wd < 360°
u* > 0.25 m s-1
stationary
z0 = 0.03 m
L < 0
Average Daily EC CO2 Flux (g m-2 d-1)
Average Daily Footprint CO2 Flux (g m-2 d-1)
700
900
1100
1300
1500
1700

Figure 10.

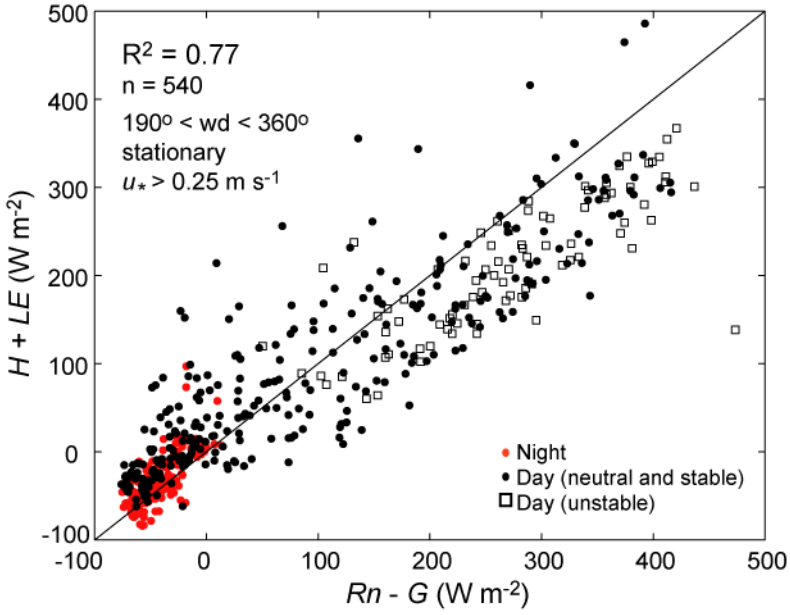
R² = 0.77
n = 540
190° < wd < 360°
stationary
u* > 0.25 m s-1
Night
Day (neutral and stable)
Day (unstable)
H + LE (W m-2)
Rn - G (W m-2)
500
400
300
200
100
0
-100
-100
0
100
200
300
400
500

Figure 11.